SPECIAL TOPICS — Acoustics

Quantitative damage imaging using Lamb wave diffraction tomography*

Hai-Yan Zhang(张海燕)[1,†], Min Ruan(阮敏)[1], Wen-Fa Zhu(朱文发)[1,2,‡], and Xiao-Dong Chai(柴晓冬)[2]

[1] School of Communication and Information Engineering, Shanghai University, Shanghai 200444, China
[2] School of Urban Railway Transportation, Shanghai University of Engineering Science, Shanghai 201620, China

(Received 5 July 2016; revised manuscript received 7 August 2016; published online 25 October 2016)

In this paper, we investigate the diffraction tomography for quantitative imaging damages of partly through-thickness holes with various shapes in isotropic plates by using converted and non-converted scattered Lamb waves generated numerically. Finite element simulations are carried out to provide the scattered wave data. The validity of the finite element model is confirmed by the comparison of scattering directivity pattern (SDP) of circle blind hole damage between the finite element simulations and the analytical results. The imaging method is based on a theoretical relation between the one-dimensional (1D) Fourier transform of the scattered projection and two-dimensional (2D) spatial Fourier transform of the scattering object. A quantitative image of the damage is obtained by carrying out the 2D inverse Fourier transform of the scattering object. The proposed approach employs a circle transducer network containing forward and backward projections, which lead to so-called transmission mode (TMDT) and reflection mode diffraction tomography (RMDT), respectively. The reconstructed results of the two projections for a non-converted S0 scattered mode are investigated to illuminate the influence of the scattering field data. The results show that Lamb wave diffraction tomography using the combination of TMDT and RMDT improves the imaging effect compared with by using only the TMDT or RMDT. The scattered data of the converted A0 mode are also used to assess the performance of the diffraction tomography method. It is found that the circle and elliptical shaped damages can still be reasonably identified from the reconstructed images while the reconstructed results of other complex shaped damages like crisscross rectangles and racecourse are relatively poor.

Keywords: Lamb waves, diffraction tomography, damage identification, Fourier diffraction theorem

PACS: 43.20.+g, 43.35.+d **DOI:** 10.1088/1674-1056/25/12/124304

1. Introduction

Lamb wave tomography is an imaging method of quantitatively assessing the size and severity of damage in plate. Early researchers[1–3] mostly used straight-ray Lamb wave (also called plate wave) tomography. However, the reconstruction algorithms used in these studies were based on the assumption of straight-ray propagation, ignoring the scattering. Malyarenko and Hinders[4] considered the diffraction effect in the time-of-flight Lamb wave tomography. They investigated the performance of time-of-flight tomography with the straight-ray assumption and the research showed that Lamb wave diffraction tomography could further improve image quality and resolution. Using finite element simulations and experiments, Belanger and Cawley[5] verified that low frequency Lamb waves could not be used for time-of-flight straight-ray quantitative tomography to evaluate the maximum depth of damage due to the invalidity of the ray theory, while the same frequency range could be used to successfully reconstruct thickness reduction in plates with diffraction tomography.[6]

With fully considering the effect of wave-damage interactions, a Lamb wave diffraction tomography approach in which the diffracted scattering field is measured to quantitatively retrieve the damage information embodies the essential development trend of Lamb wave detection. In the last decade, Lamb wave diffraction tomography based on Fourier diffraction theory has been studied for imaging flexural inhomogeneities in plates.[7–13] The scattering of plate wave by localized damage was examined within the framework of Mindlin plate theory, which provided an accurate characterisation of A0 mode at frequencies below the cut-off frequency for the A1 mode. The Born approximation for the scattered field leads to a plate-theory analog of the Fourier diffraction theorem, which relates the far-field scattering amplitudes to the spatial Fourier transform of the inhomogeneity variations. The results showed that this framework enabled the quantitative reconstructions of location, size and severity of plate damage with excellent sensitivity and offered the potential for detecting corrosion thinning, disbands and delamination damage in structural integrity management applications. However, the theoretical framework with far-field Born approximation assumed that the damage was at the center of the transducer network. In view of this, Ng[11] proposed a two-stage image approach, which overcame this limitation by first determining the location of

*Project supported by the National Natural Science Foundation of China (Grant Nos. 11474195, 11274226, 11674214, and 51478258).
†Corresponding author. E-mail: hyzh@shu.edu.cn
‡Corresponding author. E-mail: zhuwenfa1986@163.com
© 2016 Chinese Physical Society and IOP Publishing Ltd

the damage in stage-one, and then modifying the amplitudes and phases of the scattering wave signals. The amplitude and phase modification allowed the direct application of the far-field Born approximation in the stage-two damage imaging. Hence, the method was applicable for the damage at different locations with the transducer network. Most recently, Chan and Francis[12,13] have presented an extended diffraction tomography method by using numerical Green's functions. The new algorithm, built on the far-field diffraction tomography method developed by Rose and Wang,[10] overcame this far-field condition limitation and utilized a near-field multi-static data matrix as the input data. Excellent image quality has been shown for circle and racecourse shaped damages.

The above studies[7–13] only took into account a single anti-symmetric scattering mode that was the same as the incident mode. As is well known, the scattered waves also contain the converted waves when the damage is non-symmetrical about the mid-plane of the plate. The imaging effect of this converted mode has not been adequately investigated in these studies.

The purpose of this paper is to investigate the diffraction tomography for quantitative imaging damages of partly through-thickness holes with various shapes in isotropic plates by using converted and non-converted scattered Lamb waves generated numerically. The effect of the scattering wave projection on the reconstructed image quality is first inspected. The imaging results of the two scattered Lamb modes are then compared. Finally, some conclusions are drawn, which have the guidance value for Lamb wave quantitative nondestructive evaluation.

2. Fourier diffraction theorem

Given a projection $P_{\theta_i}(\boldsymbol{r})$ of the scattered field obtained by illuminating a scattering object $O(\boldsymbol{r})$ with a plane wave in the incident direction θ_i, the Fourier diffraction theorem establishes the relationship between the one-dimensional (1D) Fourier transform of the measured scattered field projection $P_{\theta_i}(\boldsymbol{r})$ and the two-dimensional (2D) Fourier transform of the scattering object $O(r)$[14] as follows:

$$F_{1D}\left\{P_{\theta_i}(\boldsymbol{r})\right\}(\omega) = F_{2D}\left\{O(\boldsymbol{r})\right\}(k_x(\omega), k_y(\omega)), \tag{1}$$

where F_{1D} and F_{2D} denote respectively 1D and 2D Fourier transforms. The theorem forms the basis of transmission and reflection mode diffraction tomography. If $P_{\theta_i}(r)$ is the forward projection, corresponding to the transmission mode diffraction tomography (TMDT), the $k_x(\omega)$ and $k_y(\omega)$ in Eq. (1) are expressed, respectively, as

$$\begin{aligned} k_x(\omega) &= \omega\cos\theta_i - \left(\sqrt{k_0^2-\omega^2}-k_0\right)\sin\theta_i, \\ k_y(\omega) &= \omega\sin\theta_i + \left(\sqrt{k_0^2-\omega^2}-k_0\right)\cos\theta_i, \end{aligned} \tag{2}$$

where θ_i and k_0 are the incident angle and the wavenumber of incident wave, respectively; ω is the angular frequency. If $P_{\theta_i}(r)$ is the backward projection, corresponding to the reflection mode diffraction tomography (RMDT), the $k_x(\omega)$ and $k_y(\omega)$ in Eq. (1) is expressed as

$$\begin{aligned} k_x(\omega) &= \omega\cos\theta_i + \left(\sqrt{k_0^2-\omega^2}+k_0\right)\sin\theta_i, \\ k_y(\omega) &= \omega\sin\theta_i - \left(\sqrt{k_0^2-\omega^2}+k_0\right)\cos\theta_i. \end{aligned} \tag{3}$$

Figure 1 gives the schematic representation of the Fourier diffraction theorem between the physical space and the k-space, where θ_i and θ_s are the incident and scattered angles, respectively. For the transmission case, the 1D Fourier transform of the forward scattered projection gives the values of the 2D Fourier transform of the scattering object along the solid semicircular arc in the k-space domain. For the reflection case, the 1D Fourier transform of the backward scattered projection gives the values of the 2D Fourier transform of the scattering object along the dash semicircular arc in the k-space domain. The two modes populate the Ewald limiting disk when incident direction θ_i changes from 0 to 2π.[15] The transmission arc populates the circle disk of radius $\sqrt{2}k$ and contains the lower spatial frequencies between 0 and $\sqrt{2}k$ as shown in Fig. 2(a). The reflection arc populates the annulus disk with inner radius $\sqrt{2}k$ and outer radius $2k$ and contains the higher spatial frequencies between $\sqrt{2}k$ and $2k$ as shown in Fig. 2(b). Figure 2(c) is the couple of the two projection modes.

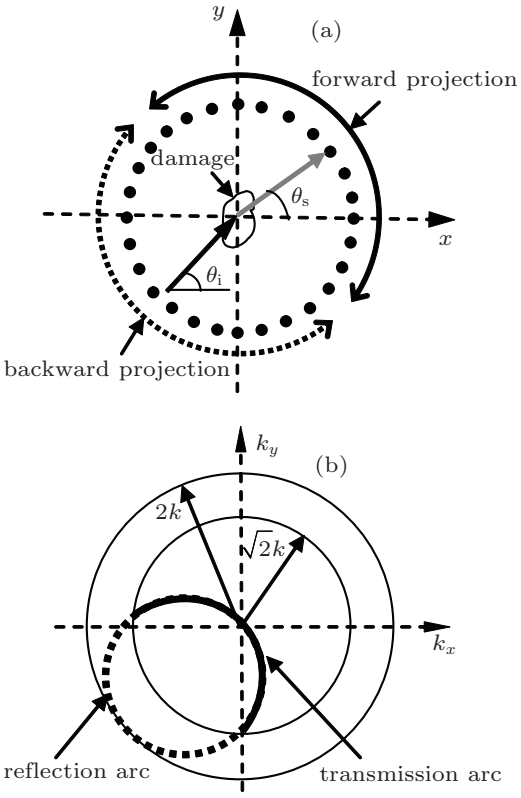


Fig. 1. Fourier diffraction theorem for forward and backward scattered waves: (a) physical space domain, and (b) k-space domain.

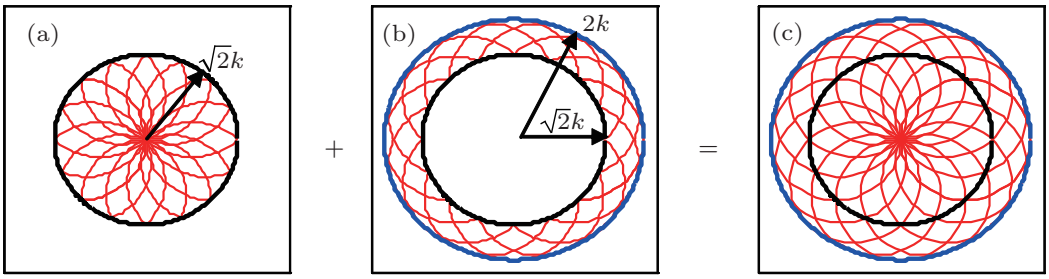


Fig. 2. (color online) Projection distributions of the 2D Fourier transform in the k-space domain: (a) forward projection, (b) backward projection, and (c) the couple of forward and backward projections.

3. Numerical modeling

3.1. Finite element model set up

In this section, numerical simulations are performed to acquire the scattered Lamb waves caused by the damages. The numerically simulated data of different damage cases are then used as the input to a diffraction tomography algorithm for quantitative damage imaging. A commercial finite element (FE) analysis package PZFlex is adopted for the simulations. A server Intel Xeon CPU E5-2650 with 128 GB RAM is used to perform all FE calculations.

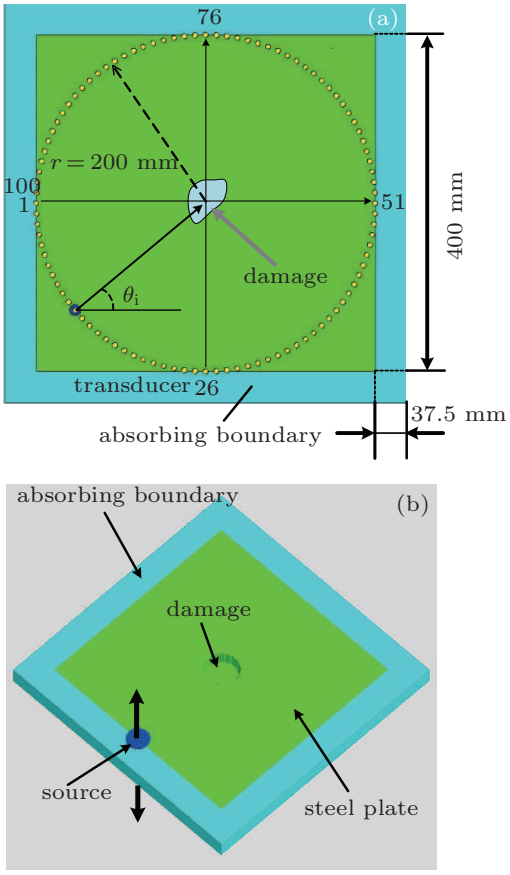


Fig. 3. (color online) Schematic diagrams of the configuration used in the finite element simulations: (a) transducer network and (b) excitation of the S0 mode.

Consider the case of a square steel plate with thickness 2 mm and side 475 mm, Young's modulus 210 GPa, density 8100 kg/m^3, and Poisson's ratio 0.33. The damage is located in the center of the plate. The plate is interrogated by a tone-burst of center frequency 200 kHz applied to the elements of a circular transducer array with the radius 200 mm, which are surrounded by an absorbing region with side 37.5 mm to prevent unwanted reflections from the edge of the plate. With this combination of frequency and thickness, the fundamental S0 mode is excited by exerting symmetric normal displacements at the same location on the opposite sides of the plate. The schematic diagram of the finite element setup showing the transducer array and excitation mode is shown in Fig. 3. The array contains 100 transducers, marked as 1–100. During the interrogation of the plate, one transducer is excited with a 5-cycle Hanning windowed tone-burst signal shown in Fig. 4, while all transducers (including the exciting transducer) receive the resulting response.

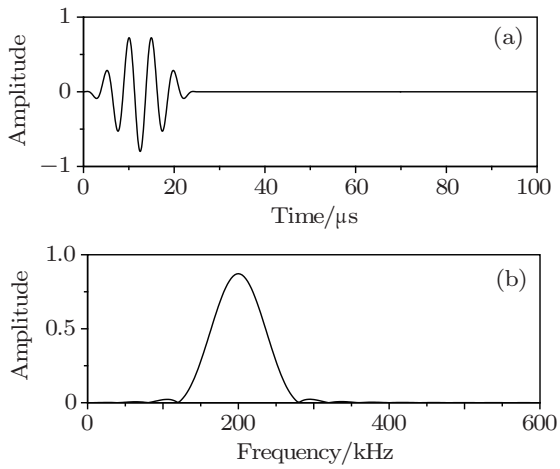


Fig. 4. The 5-cycle tone burst: (a) original time–domain signal; (b) frequency–domain signal.

The plate is modeled into four regions, which are shown in Fig. 5. Region I includes the damage, in which the element size is 0.357 mm × 0.357 mm × 0.333 mm. Regions II and III are around the damage, in which the element sizes are 0.714 mm × 0.357 mm × 0.333 mm and 0.357 mm × 0.714 mm × 0.333 mm, respectively. Region IV is outside the damage, in which the element size is 0.714 mm × 0.714 mm × 0.333 mm. Thus, the grids around the damage are relatively close to allow high precision in describing the damage, while

the grids outside the damage are sparse to speed up the calculation. These regions are all modelled by hexahedral elements. The total number of elements in the finite element model is $711 \times 711 \times 6 = 3033126$. Diligent and Lowe[16] have demonstrated that two or three elements through the thickness are enough to model the waves with low frequency and simple mode shapes. Therefore, 6 elements in the thickness direction meet the requirements. Also, the time interval for each finite element simulation is 200 μs, using a small enough time step of 17 ns.

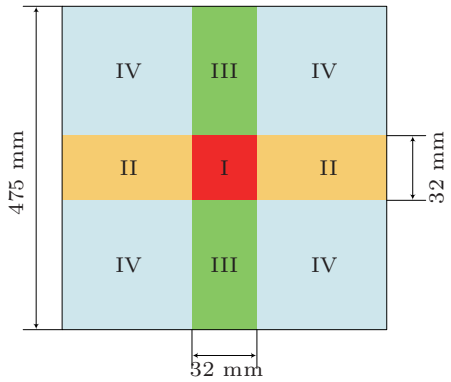


Fig. 5. (color online) Region partition in the finite element model.

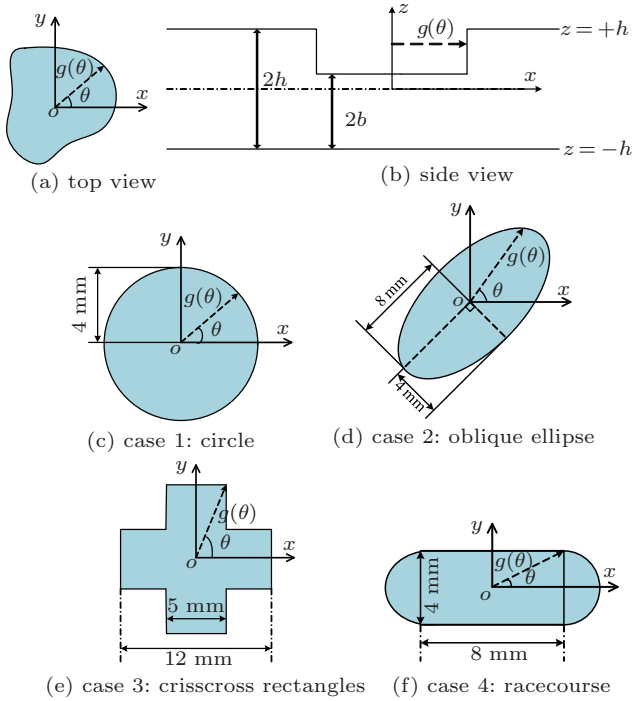


Fig. 6. (color online) Schematics of damages with different shapes and sizes.

The damage is modeled as a non-symmetric cavity about the mid-plane of the plate as shown in Figs. 6(a) and 6(b). The plate thickness is $2h$ and the thickness under the cavity is $2b$. The surfaces of the plate and the cavity are assumed to be traction free. Four damage cases are considered in this study. They consist of different shapes and sizes to comprehensively verify the capacity of the diffraction tomography method. Defining the center of the transducer network as the origin, the shape and size for each case are shown in Figs. 6(c)–6(f).

3.2. Validation of finite element model

This section gives an analytic verification of the three-dimensional (3D) finite element model. The analytical model for guided wave scattering from a circle blind hole damage in an isotropic plate by using Poisson and Mindlin plate wave theories was presented by Cegla *et al.* in Ref. [17]. In this model the wave function expansion technique and coupling conditions at the defect boundary were used in order to evaluate the scattered far fields of the three fundamental guided wave modes. The results will be compared with those of the finite model where the circle blind hole damage with radius $a = 4$ mm and hole depth $2(h-b) = 1.6$ mm in case 1 is used in the validation.

As is well known, the mode conversion phenomena will occur when the incident S0 Lamb mode interacts with the non-symmetric damage. There will be S0, converted A0 and SH0 mode waves in the scattering fields at frequency-thickness product 400 kHz · mm. Each mode exists in a dominating displacement component in the far field. The scattered S0, A0, and SH0 modes can be captured by calculating the radial in-plane displacement u_r, tangential in-plane displacement u_θ, and out-of-plane displacement u_z, respectively. The scattering far field amplitudes in the polar coordinate system are here defined as follows:[18]

$$\begin{aligned} u_r &= u_x \cos\theta_s + u_y \sin\theta_s, \\ u_{SH0} &= u_{\theta_s} = u_x \sin\theta_s - u_y \cos\theta_s, \quad u_z = u_z, \end{aligned} \tag{4}$$

where θ_s is the scattering angle of the scattered Lamb wave, and u_x, u_y, u_z are scattering far field amplitudes in the cartesian coordinate system, respectively. In the finite element simulation, the displacement components u_x, u_y, u_z on the upper surface of the plate are extracted.

Two finite element simulations with identical grids for the plate with and without the damage are conducted. The scattered Lamb waves are obtained from 100 monitoring locations by calculating the difference between the signals from the intact and the damage plates. The scattering directivity pattern (SDP) is obtained by calculating the maximum absolute amplitude of the scattered Lamb waves, where the amplitudes of all scattered waves are normalized by the maximum amplitude of the incident S0 Lamb wave at the center location of the damage zone of the incident intact plate. As observed in Fig. 7, simulations agreed well with analytical results, confirming the validity of the finite element model. The red solid curves are the results calculated from the analytical model described in Ref. [17] and blue dotted lines are the results of the finite simulations.

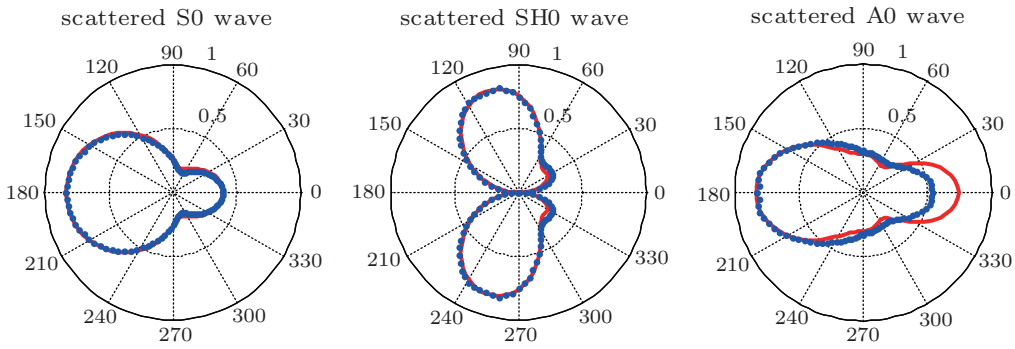


Fig. 7. (color online) Analytical (red solid curves) and finite element simulation (blue dotted curves) results for circle blind hole damage with radius $a = 4$ mm and hole depth $2(h - b) = 1.6$ mm at frequency-thickness product 400 kHz·mm.

3.3. Reconstructions of damages with different shapes by direct Fourier inversion

Using the analytically verified 3D finite element scattering model, the scattered S0 and A0 Lamb waves for damages of different shapes and sizes can then calculated. For a fixed incident wave angle θ_i, the scattered waves at various scattered angles θ_s provide values of 2D Fourier transform of scattering object in a semi-circle in the k-space domain. The scattered data are taken at 100 monitoring nodes located at $r = 200$ mm and $0^\circ \leq \theta_s \leq 360^\circ$ in steps of 3.6°. Diffraction tomography requires enough projection angles to populate throughout the circle or annulus region in the k-space domain,[19] which can be obtained by varying the incident wave angle θ_i. In the subsequent image reconstruction, 16 projection angles in steps of 22.5° for $0^\circ \leq \theta_i \leq 360^\circ$ are used.

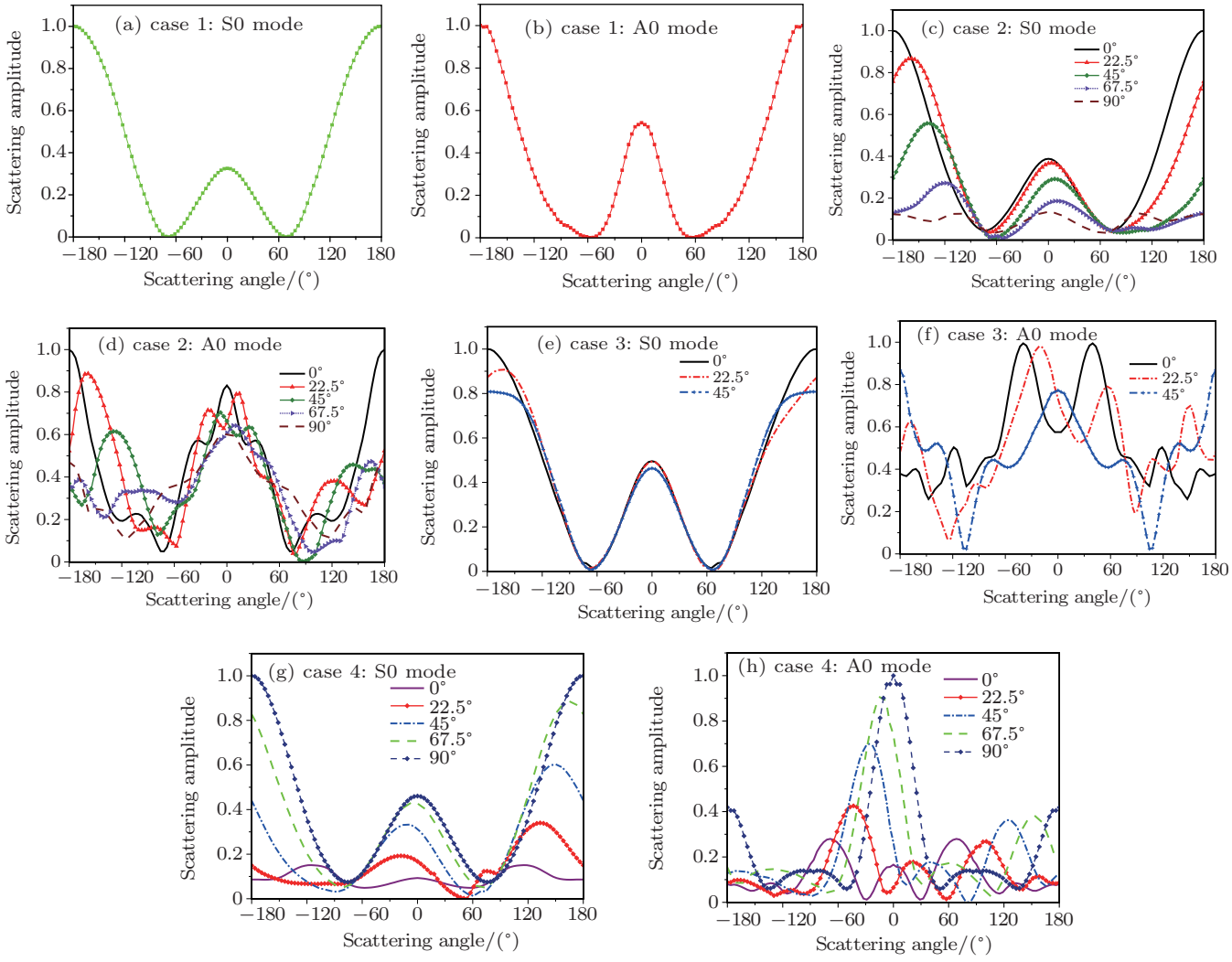


Fig. 8. (color online) Scattered S0 and A0 Lamb wave data of four damage cases in Fig. 6 for different incident directions θ_i, panels (a), (c), (e), (g): S0 mode; panels (b), (d), (f), (h): A0 mode.

Scattered S0 and A0 Lamb wave data of four kinds of damages in Fig. 6 for different incident angles are shown in Fig. 8. Due to the geometric symmetry of the damage, we just need to collect the scattered data of those symmetrical projection directions. As seen in Figs. 8(a) and 8(b), one incident angle is sufficient for circle shaped damage. For elliptical, rectangular, racecourse shaped damages, scattered data from 5, 3, and 5 projection angles are acquired, respectively, as shown in Figs. 8(c)–8(h).

The quantitative images of the damages are evaluated by carrying out the 2D inverse Fourier transform for the obtained $F_{2D}\{O(r)\}(k_x(\omega),k_y(\omega))$. Because the scattered wave data must be cast on a uniform calculation grid in k-space domain before the 2D inverse Fourier transform, a bilinear interpolation technique is employed in the 2D Fourier interpolation.

The numerical simulated data of the four cases in Fig. 8 are used as the input data of the diffraction tomography. The scattered waves contain forward and backward projection data, which lead to the so-called transmission mode (TMDT) and reflection mode diffraction tomography (RMDT), respectively.[14] The reconstructed results of the two projection data for S0 mode are first investigated to illuminate the influence of the scattering field projection. Then, the scattered full field data of the converted A0 mode are used to assess the performance of the diffraction tomography method in the presence of the mode conversion.

Figures 9–12 show the reconstructed images of four cases by using the scattered field data of S0 mode. The black circle indicates the true damage shape and size. The figures illustrate that both TMDT and RMDT give bad estimates for the size and shape of different damages. Therefore, Lamb wave diffraction tomography cannot provide better reconstruction results by using only the forward or backward projection data. However, the combination of TMDT and RMDT enhances the image quality. The reconstructed and true damages are shown to be in good agreement in Figs. 9(c)–12(c) when using the full field scattered data. Even for the complex shaped damages like crisscross rectangles and racecourse as seen in Figs. 11(c)–12(c), the method is also very suitable.

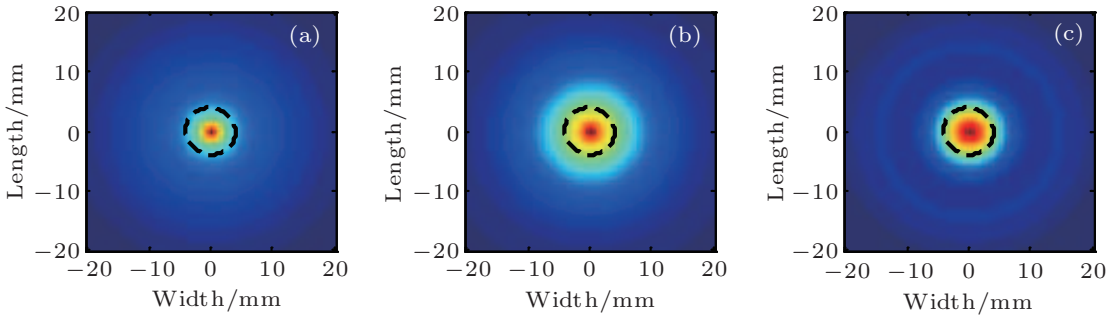


Fig. 9. (color online) Reconstructed images of the damage in case 1 with using the scattered data of S0 mode as the input of diffraction tomography: (a) forward scattered data, (b) backward scattered data, and (c) full field scattered data.

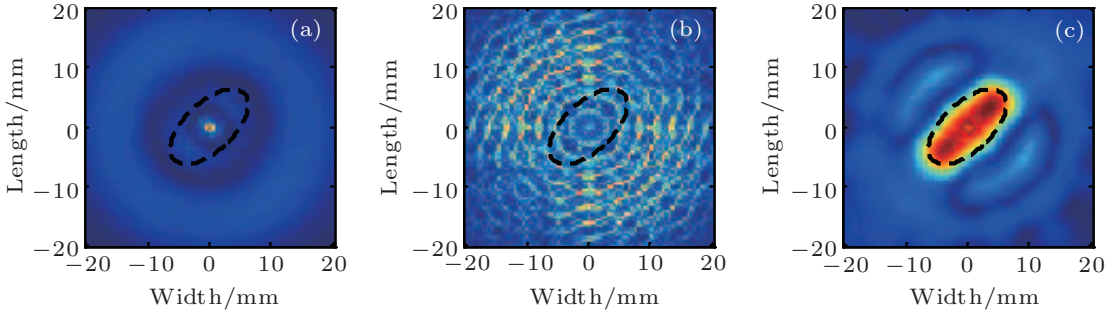


Fig. 10. (color online) Reconstructed images of the damage in case 2 with using the scattered data of S0 mode as the input of diffraction tomography: (a) forward scattered data, (b) backward scattered data, and (c) full field scattered data.

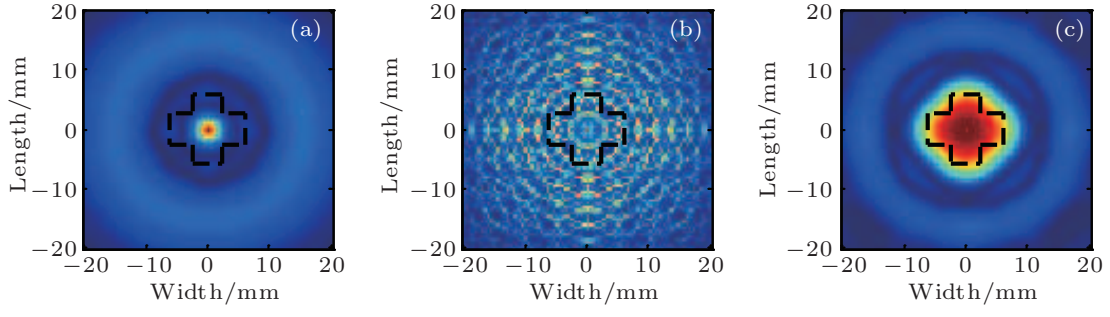


Fig. 11. (color online) Reconstructed images of the damage in case 3 with using the scattered data of S0 mode as the input of diffraction tomography: (a) forward scattered data, (b) backward scattered data, and (c) full field scattered data.

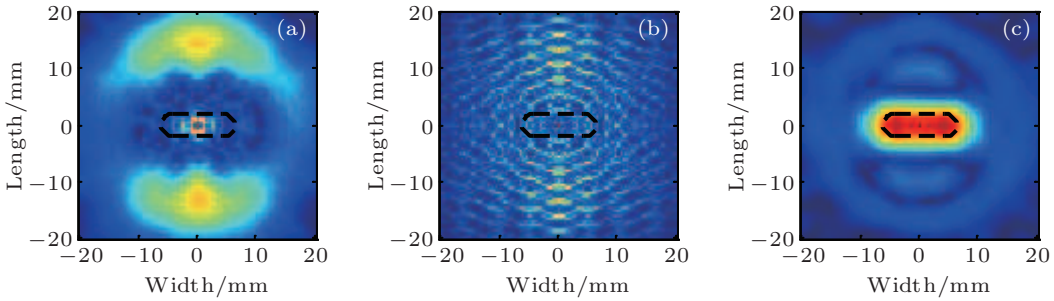


Fig. 12. (color online) Reconstructed images of the damage in case 4 with using the scattered data of S0 mode as the input of diffraction tomography: (a) forward scattered data, (b) backward scattered data, and (c) full field scattered data.

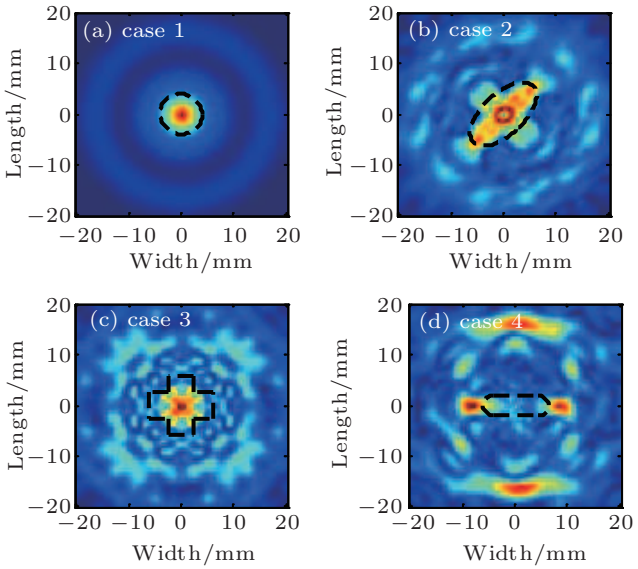


Fig. 13. (color online) Reconstructed images of four cases with using the full field scattered data of A0 mode as the input of diffraction tomography.

Figure 13 shows the reconstructed images of four damage cases with using the full field scattered data of A0 mode as the input of diffraction tomography. It can be seen that the circle and elliptical damages can still be reasonably identified from the reconstructed images. However, the reconstructed results of other complex shaped damages like crisscross rectangles and racecourse are relatively poor.

4. Conclusions

An imaging approach based on Fourier diffraction projection theorem is investigated for quantitatively characterizing various shaped damages in plate-like structures. Unlike the existing Lamb wave diffraction tomography method that is based on Mindlin plate theory for imaging inhomogeneity with symmetric reduction of plate thickness, this paper focuses on the partly through-thick holes with various shapes that are not symmetric about the mid-plane of the plate, for which the scattered waves will also contain the converted antisymmetric mode although a symmetric S0 incoming field is considered. Using the full field scattered S0 wave data generated from the finite simulations, imaging results for four damage cases with different shapes like circle, inclined ellipse, crisscross rectangles and racecourse show excellent image quality. The predicted geometrical shapes and sizes of the damages in the four numerical examples are highly accurate and comparable to the actual damage characteristics. However, both TMDT and RMDT using the only forward or backward projections cannot provide good estimates for the shape and size of damage because they lose the detailed information about the image. The imaging results of the converted A0 mode for these damages are also observed. It is found that the complex shaped damages are not well reconstructed except for the circle and elliptical damages. The results in this paper illustrate that the mode-converted scattered Lamb waves can also be used for quantitatively imaging simple shaped damages.

References

[1] Jansen D P and Hutchins D S 1992 *Ultrasonics* **30** 245
[2] MCKeon J C P and Hinders M K 1999 *J. Acoust. Soc. Am.* **106** 2568
[3] MCKeon J C P and Hinders M K 2000 *J. Acoust. Soc. Am.* **108** 1631
[4] Malyarenko E V and Hinders M K 2001 *Ultrasonics* **39** 269
[5] Belanger P and Cawley P 2009 *NDT & E International* **42** 113
[6] Belanger P, Cawley P and Simonetti P F 2010 *IEEE Trans. Ultra Ferr. Freq. Control* **57** 1405
[7] Wang C H and Rose L R F 2003 *Rev. Quantum Nondestr. Eval.* **22** 1615
[8] Rohde A H, Vedit M, Rose L R F and Homer J 2008 *Ultrasonics* **48** 6
[9] Rohde A H, Rose L R F, Vedit M and Wang C H 2009 *Mater. Forum* **33** 489
[10] Rose L R F and Wang C H 2010 *J. Acoust. Soc. Am.* **127** 754
[11] Ng C T 2015 *Earthquakes and Structures* **8** 821
[12] Chan E, Rose L R F and Wang C H 2015 *Ultrasonics* **59** 1
[13] Rose L R F, Chan E and Wang C H 2015 *Wave Motions* **58** 222
[14] He N, Tao J X and Xua S J 2010 *Procedia Enginnering* **7** 51
[15] Simonetti F, Huang L, Duric N and Littrup P 2009 *Med. Phys.* **36** 2955
[16] Diligent O and Lowe M J 2005 *J. Acoust. Soc. Am.* **118** 2869
[17] Cegla F B, Rohde A H and Veidt M 2008 *Wave Motion* **45** 162
[18] Zheng Y and Zhou J J 2014 *Engineering Mechanics* **31** 21
[19] Rohde A H, Veidt M, Rose L R F and Homer J 2008 *Ultrasonics* **48** 6